RSC Advances

ROYAL SOCIETY OF CHEMISTRY

www.rsc.org/advances

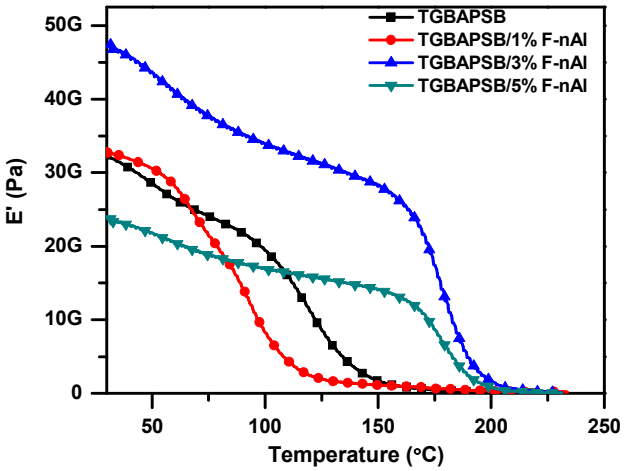

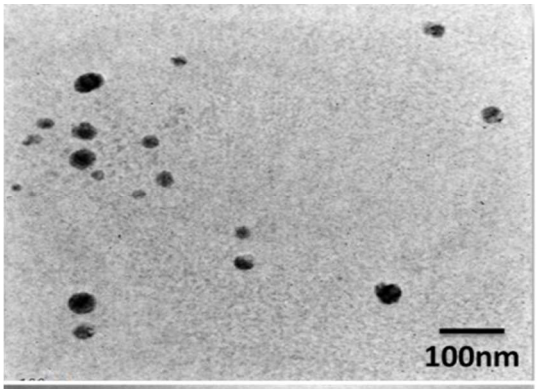

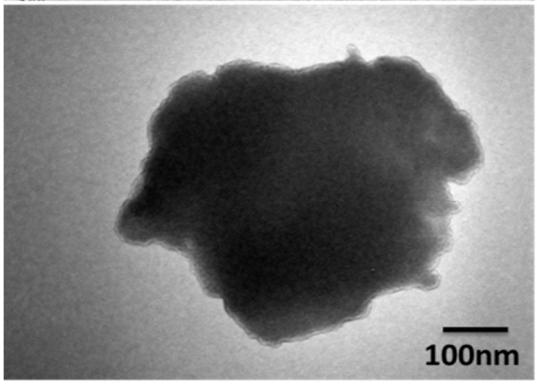

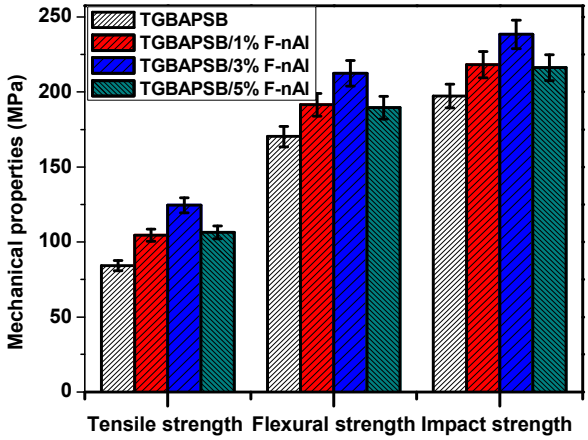

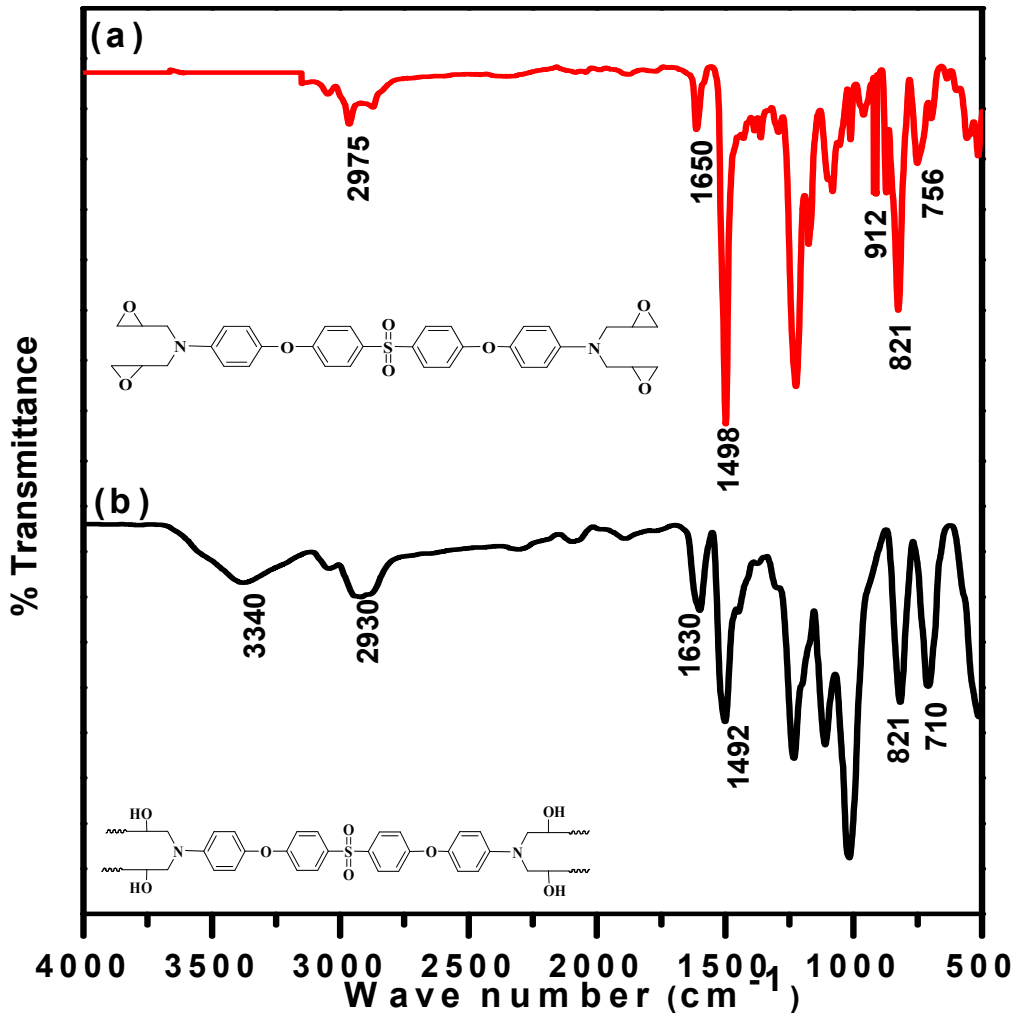

Fig. 3.

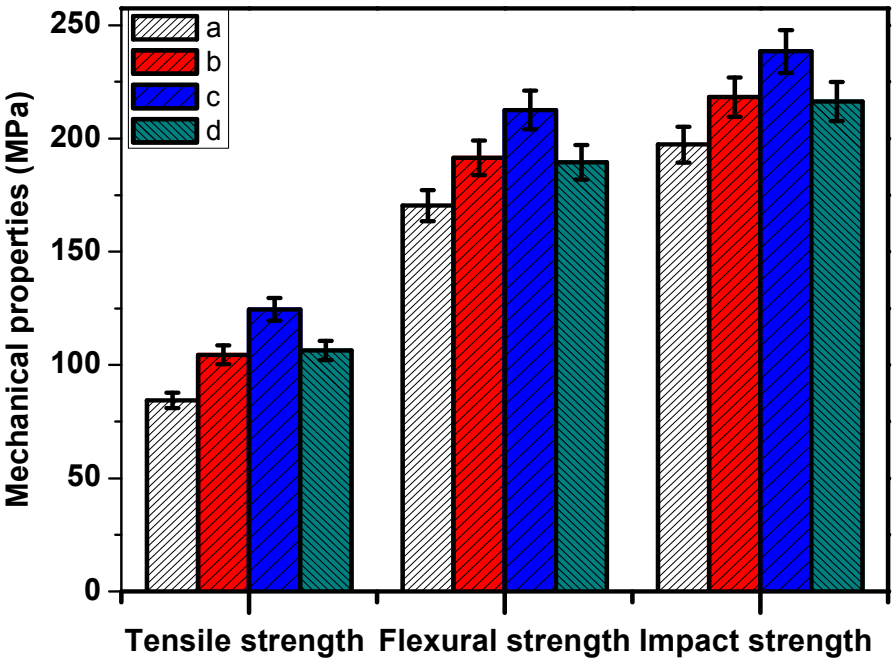

Fig. 11.

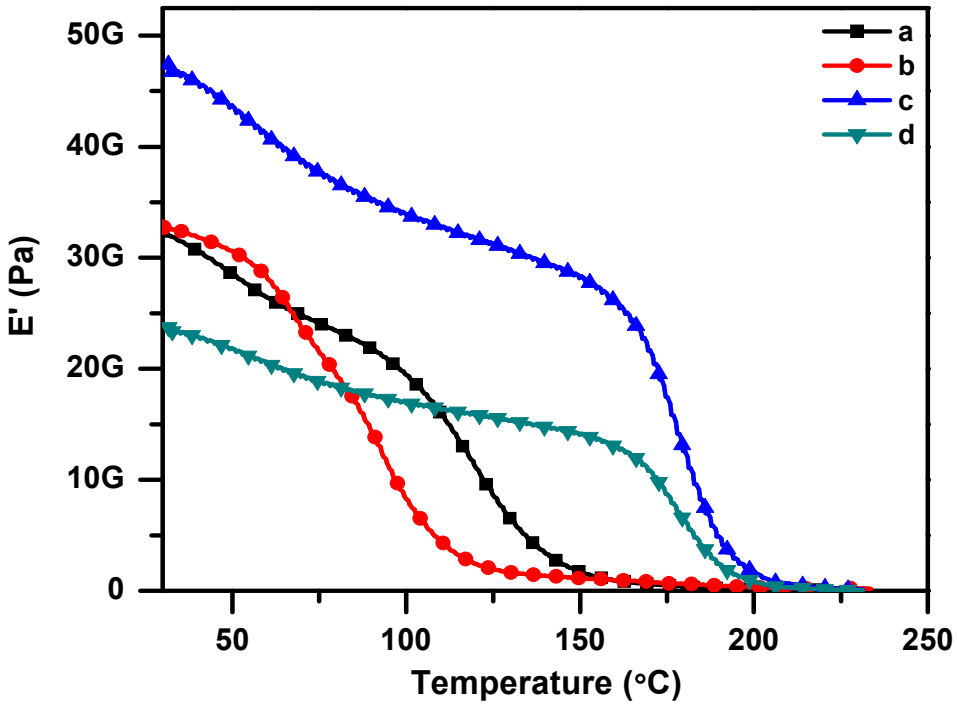

Fig. 12.

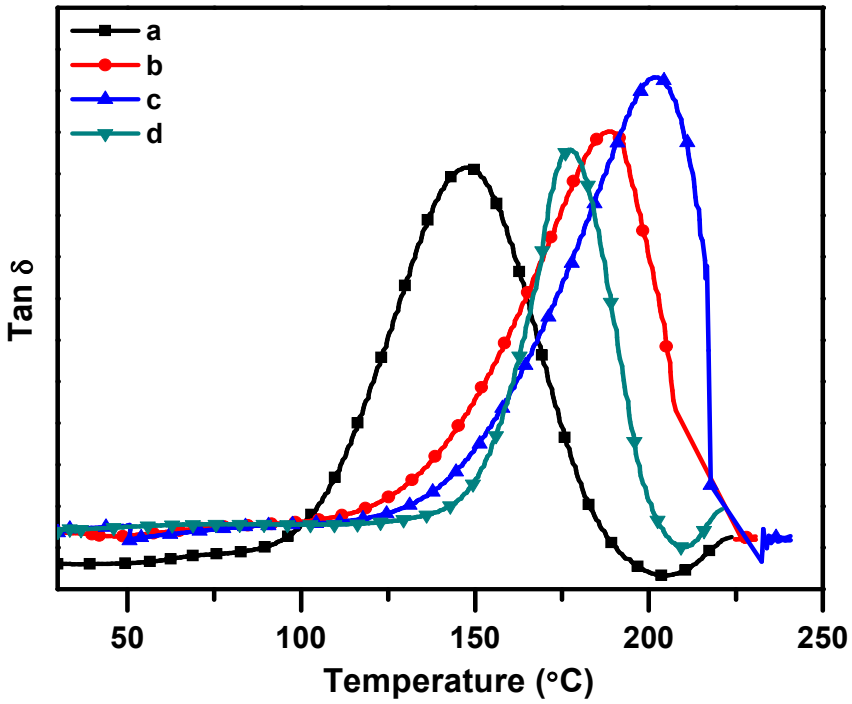

Fig. 13.

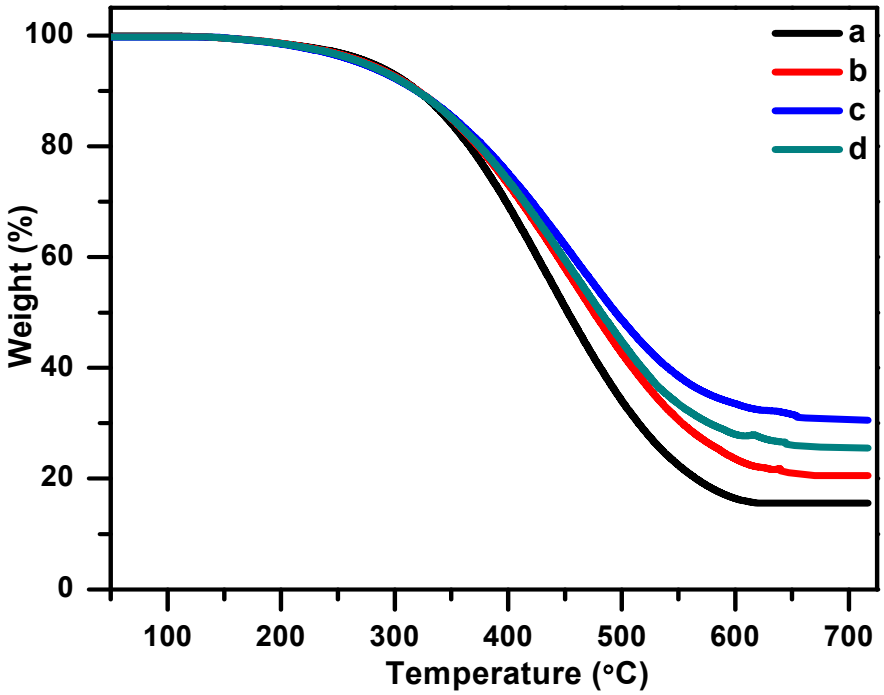

Fig. 14.

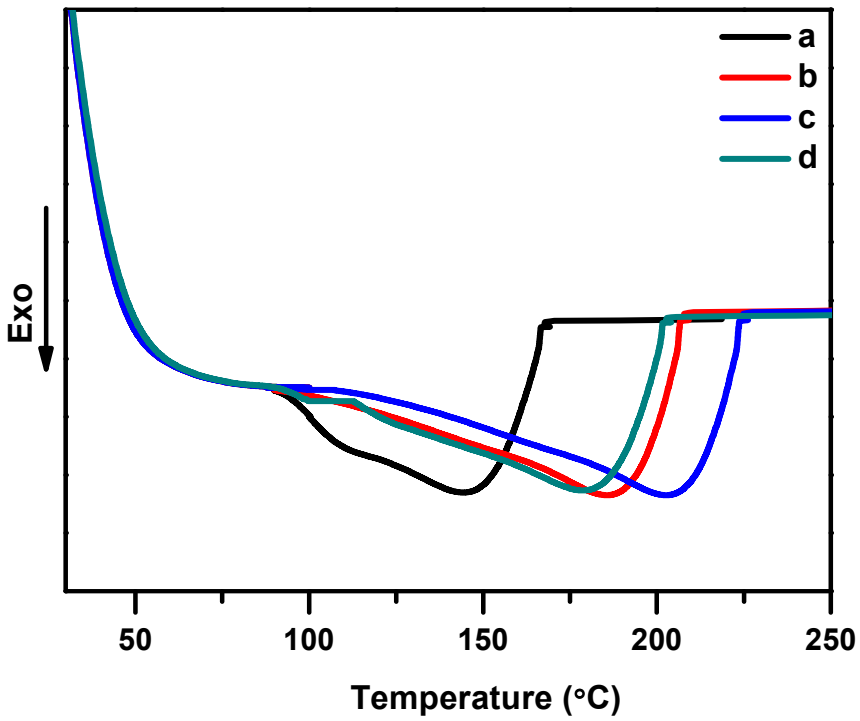

Fig. 15.

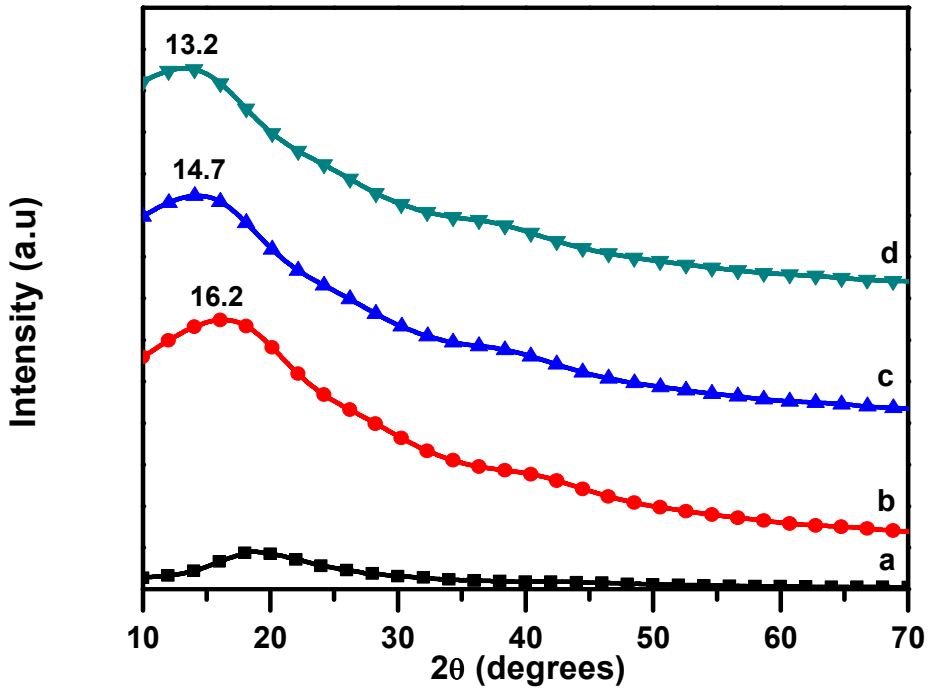

Fig. 16.

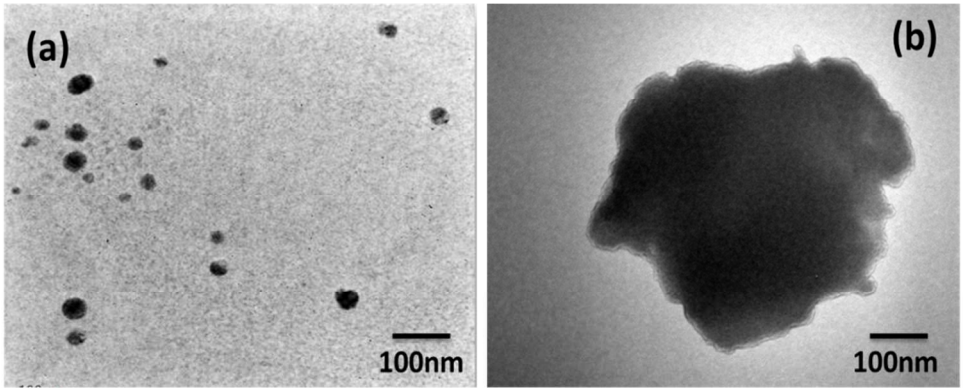

Fig. 17.

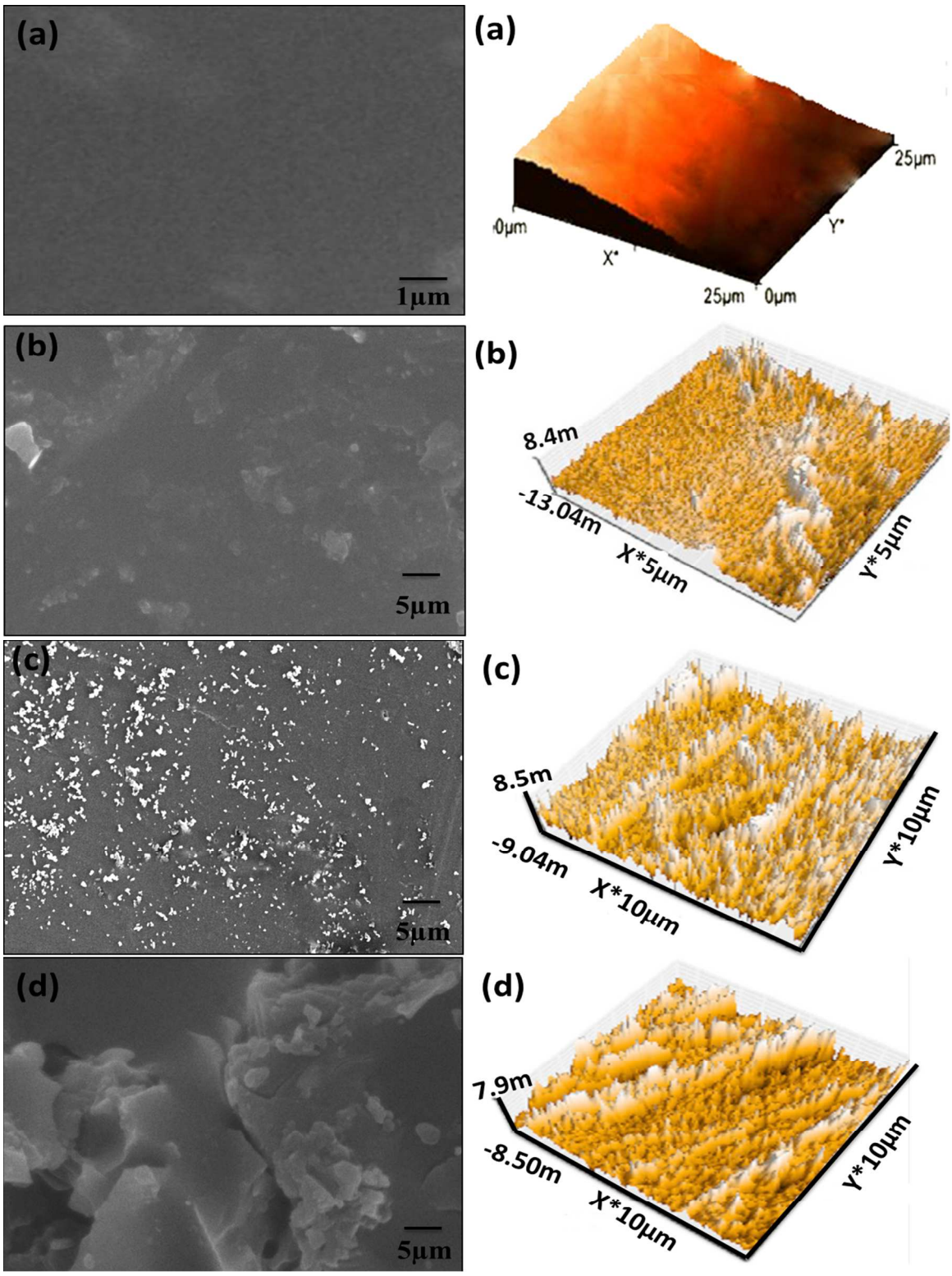

Fig. 18.

Studies on mechanical, thermal and dynamic mechanical properties of functionalized nanoalumina/reinforced sulphone ether linked tetra glycidyl-toughened epoxy nanocomposites

D. Duraibabu[a], M. Alagar[b] and S. Ananda Kumar[a]*

[a]Department of Chemistry, Anna University, Chennai 600025, India.

[b]Department of Chemical Engineering, Anna University, Chennai 600025, India.

*sri_anand_72@yahoo.com

Tel. No: +91 44-22358661. Fax. No: 91-44-22200660

ABSTRACT

The objective of the present work is to synthesize 1,4'-bis (4-amine-phenoxy) sulphone benzene epoxy resin (TGBAPSB) via 1,4'-bis (4-amine-phenoxy) sulphone benzene (BAPSB) and epichlorohydrin in order to obtain tetra functional epoxy with improved properties. The molecular structure of TGBAPSB epoxy resin was confirmed from FTIR and NMR spectral data and molecular weight was determined by GPC and epoxy equivalent weight (EEW) by titration method. The amine functionalized nanoalumina (F-nAl) was synthesized via the solgel method using 3-aminopropyltriethoxysilane and has been confirmed by FT-IR. TGBAPSB epoxy resin was further reinforced with varying weight percentages (1-5wt %) of F-nAl and cured with diaminodiphenylmethane (DDM). Thermal and thermo-mechanical behaviour of TGBAPSB epoxy matrix and nanocomposites were analysed by TGA, DMA and DSC. The surface morphology of the epoxy nanocomposites was examined using XRD, TEM, SEM and AFM studies. Data obtained from the mechanical, thermal and thermo-mechanical, dielectric and water absorption studies indicate a significant improvement in properties of the resultant epoxy nanocomposites, which appear to be an ideal candidate for advanced high performance applications when compared to those of neat epoxy matrix.

Key words: Sulphone epoxy resin, mechanical properties, thermal properties, nanocomposites, morphology.

1. Introduction

The characteristics of tetra glycidyl epoxy resins constitute an excellent combination of chemical and corrosion resistance, and good mechanical and electrical properties. These characteristics, along with a long service life, make epoxies a necessity in the future growth of new technologies. Presently, there is high potential for more sophisticated application of tetra functional epoxies in both automotive and aerospace industries. However, these epoxies have brittle characteristics that prevent their use in such potential applications in aerospace and automotive industries. For structural applications, for example, epoxy resins tend to be either brittle or notch sensitive. Therefore, tremendous efforts have been focused on improving the toughness of epoxy systems, which has stimulated an overwhelming interest in the recent decades.[1-3] Toughening can be achieved by reduction of cross-link density or by the use of liquid rubbers and plasticizers leading to an increased plastic deformation. However, none of these methods seems to have improved the toughness of epoxies without the loss of rigidity.[4-9] Quite recently, epoxy resins have been modified with materials having rigid and soft skeleton in order to have both toughness and stiffness that are ideally required for high performance applications.[10-13] It has also been reported that the toughness of tetra functional epoxy resin can be improved without a significant loss of stiffness by skeletal modification through the incorporation of specific atoms and groups into their backbone in order to meet the required high performance characteristics mentioned above. Though the literature describes a variety of epoxy resins and their nanocomposites, there is still a need for high performance tetraglycidyl epoxy resins having stiffness and toughness and their demand is increasing day by day. Hence, structural modification of epoxy resins along with suitable nanoreinforcements to achieve enhanced thermal and thermo mechanical properties is required for high performance industrial applications.[14-17] Introduction of sulphur group in to epoxy resins offers excellent thermal stability, high moisture resistance, low ionic contaminant concentration, and good dielectric properties. The addition of inorganic nanoparticles, carbon nanotubes and carbon flakes are the widely used as nanometric reinforcements for epoxy matrices to enhance their mechanical behavior.[18] However, it has been reported recently that alumina nanoparticles emerged as potential nanoreinforcement for an advanced composite insulation materials when compared to that of micron size filled alumina powder.[19] Therefore the development of novel skeletal modified tetraglycidyl epoxy resins having both toughness and stiffness is a major goal in the

field today. To achieve both toughness and stiffness to a greater extent, tetra functional epoxy resin is skeletally modified with sulphone moiety and subsequently reinforced with optimum percentage of functionalized inorganic nanomaterial (F-nAl) and cured with DDM. Hence an attempt to achieve the above said objectives is reported here with supporting evidences.

2.0 Experimental

2.1 Materials

All chemicals were used without further purification except dimethylformamide (DMF) which was purified by distillation under reduced pressure over calcium hydride. *p*-chloronitrobenzene, potassium carbonate, absolute ethanol, hydrazine hydrate (80 wt% water solution), epichlorohydrin (EPC), benzene, tetrahydrofuran (THF), dimethylbenzene and sodium hydroxide were obtained from SD Fine Chemical Company, India. Alumina nanoparticles, di-hydroxy diphenylsulphone and 3-aminopropyltriethoxysilane (APTES) were purchased from Sigma Aldrich, India. 4, 4'-diaminodiphenylmethane (DDM) was obtained from Huntsman, USA.

2.2 Synthesis of (4-nitro-phenoxy) sulphone benzene (BNPSB) and (4-amine-phenoxy) sulphone benzene (BAPSB)

BNPSB was synthesized by the reaction of di-hydroxy diphenylsulphone (0.20 mol) and *p*-chloro nitrobenzene (0.44mol) in DMF (300 ml) in the presence of potassium carbonate (0.44mol). The reactants were heated to 145–150°C for 8–10 h under N_2 atmosphere. After being cooled to room temperature, the resulting product was poured into a water/ethanol (1/1, v/v) solution and filtered to get a yellow colour solid product, which was recrystallized from ethanol. BNPSB (0.20 mol), 0.78g Pd/C and 600 ml ethanol were introduced into a 1000 ml three-neck flask to which hydrazine hydrate (85 wt%) was added in dropwise over a period of 1 h at reflux temperature and the reaction continued for about 5 h. The product BAPSB obtained was purified and preserved for further use.[20] The sequence of reactions involved is illustrated in Scheme 1.

2.3 Synthesis TGBAPSB epoxy resin

Tetraglycidyl (4-amine-phenoxy) sulphone benzene (TGBAPSB) resin was synthesized using EPC and BAPSB with 40% NaOH solution.[20] A pale brown coloured resin TGBAPSB obtained (yield 80%) was purified and preserved for further use (Scheme 1).

2.4 Amino functionalized nano alumina

Al_2O_3 nanoparticles were dried in a vacuum oven at 180°C for 24 h to remove the moisture adsorbed on the surface. 4 g of Al_2O_3 nanoparticles and an appropriate amount of 3-aminopropyltriethoxysilane (4.4g) were added into a 500 ml three-neck flask, equipped with a mechanical stirrer and a reflux condenser, and are mixed in high purity dimethylbenzene by stirring at 110–120°C for at least 4 h. After filtration, the APTES functionalized Al_2O_3 nanoparticles were washed several times with dimethylbenzene to remove the unreacted silane moieties and dried in a vacuum oven at 120°C for 2 h to remove the residual solvent.[21] The sequence of reactions involved is illustrated in Scheme 2.

2.5 Preparation of surface-modified nanoalumina reinforced epoxy nanocomposites

The TGBAPSB epoxy resin and the desired amount of 1, 3 and 5wt% of amino functionalized nanoalumina were mechanically stirred at 50ºC for 24h. A stoichiometric amount of DDM, corresponding to epoxy equivalents was also added (Table S1). The resulting product was poured into a preheated mould. The mould was preheated at 120 ºC for 1h to remove the moisture and trapped air. The samples were cured successively at 120 ºC for 2 h, post-cured at 180 ºC for 3 h and finally the cured sample was removed from the mould and characterized. The functionalized nanoalumina (F-nAl) forms a covalent bond with TGBAPSB epoxy resin as shown in Scheme 3.

26. Characterization

FT-IR spectra were recorded on a Perkin Elmer 781 FTIR spectrometer to determine the chemical structure of TGBAPSB epoxy resin. The spectrum of TGBAPSB epoxy resin cured with DDM was obtained by the following method. A small portion of the cured epoxy matrix was ground to a fine powder, mixed with KBr powder, and pressed into a pellet which is used to obtain the spectrum. ^{1}H and ^{13}C NMR spectra were recorded on a Bruker 400-MHz NMR spectrometer with $CDCl_3$ as the solvent as internal reference and TMS as external reference. The dynamic mechanical analysis was carried out on SII Nanotechnology (Model DMS-6000 Japan) in a three point bending configuration, at a temperature range of 30 to 250°C using a specimen with the dimension of 55mm×10mm×3mm. The frequency used with 1.0Hz at rate is 2°C min^{-1} for cure epoxy nanocomposites. The instrument measured the storage modulus (E′) and dumping (tan δ) of the specimen under on oscillatory load as a function of temperature. The temperature corresponding to the maximum in tan δ versus temperature plots was recorded as the measurement of glass transition temperature (T_g). Thermo gravimetric analysis of composites was carried out using TGA - Thermal Analyst NETZSCH STA 409 PC (TA instruments USA) at a heating rate of 10°C/min from 0°C to 700°C under a continuous flow of N_2 atmosphere (60mL/min) to determine thermal degradation temperature, percentage weight loss and char yield formation. The instrument was calibrated with calcium oxalate and aluminum supplied by NETZSCH. About 50mg of samples was taken for each analysis. X-ray diffraction (XRD) studies of the samples were carried out using a Rich Saifert-3000. X ray diffractometer CuKα radiation with a Copper target (λ 1.5405 Å) over the 2θ range of 10-70° at a scanning rate of 0.04°/min. A JEOL JSM-6360 Scanning electron microscope (SEM) was used for the sample analysis and the fractured samples were prepared by coating gold on the surface of the samples and analyzed further. A JEOL JEM-3010 analytical transmission electron microscope (TEM), operating at 300 kV with a measured point-to-point resolution of 0.23nm, was used to characterize the phase morphology of the polymers. TEM samples were prepared by dissolving polymers in DMF mounted on carbon-coated Cu TEM grids and dried 24h at room temperature (RT) to form a film in <100 nm size. The surface topology of the fractured surface was investigated by means of AFM Seiko SPI3800N, series SPA-400 (Tokyo, Japan). The surface roughness of the samples was analyzed. The dielectric constant measurements were carried out with help of impedance analyser (Solartron impedance/gain

phase analyser 1260) at room temperature (RT) using platinum (Pt) electrode at 30°C at a frequency range of 1 MHz. This experiment was repeated four times at the same condition.

2.7 Gel permeation of chromatography (GPC)

The number average molecular weight ($\bar{M}_n$),weight average molecular weight ($\bar{M}_w$) and polydispersity index ($\bar{M}_w/\bar{M}_n$) of the epoxy samples were determined with Waters 501 gel permeation chromatography equipped with three ultra styragel columns and a differential refractive index (RI-401) detector. The molecular weights were calibrated against polystyrene standards using tetrahydrofuran as mobile phase.

2.8 Determination of the epoxy equivalent weight (EEW) of the tetra glycidyl epoxy resin

The EEW determination was performed using the pyridine/hydrochloride titration method and the experimental result obtained was 176 (g/eq.) which is close to the theoretical value of 164 (g/eq). About 2 to 3 g of the TGBAPSB epoxy resin was weighed in a 250ml round bottom flask. 25ml of 0.2N pyridinium chloride (4ml of concentration hydrochloric acid in 246 ml of pyridine) was added. Then the flask was gently heated and refluxed for 30 min continuously and cooled. Then 0.1N of methanol and a few drops of phenolphthalein were added, titrated against 0.2N NaOH. Blank titration was also carried out. The EEW value of the tetra glycidyl compound was determined using the following equation (1).

$$EEW = (10000\ W)/(f\ (B-S)) \quad (1)$$

Where,

W= the weight of tetra glycidyl epoxy resin (g)

f= the calibration factor for NaOH solution

B= the amount of NaOH solution for blank test (ml)

S= the amount of NaOH solution for tetra glycidyl epoxy resin sample (ml)

2.9 Mechanical properties

The tensile, (stress–strain) properties were determined using INSTRON (Model 6025 UK) as per ASTM D 3039 at 10 mm/min cross-head speed using specimen with a width of 25 mm, length of 200 mm, and thickness of 3 mm. A distance of 115mm was kept in between the grips. The flexural (strength and modulus) properties were measured (INSTRON, Model 6025 UK) as per ASTM D 790 using specimen with dimensions 3 mm in depth, 10 mm in width, and 90 mm in length at 10 mm/min cross-head speed. The unnotched Izod impact strength of each sample was studied as per ASTM D 256-88. All the samples were tested unnotched so that they would be more sensitive to the transitions between ductility and brittleness. Specimens, having a thickness of 3.2mm with 10mm cross section and 64 mm length were clamped in the base of the pendulum testing machine so that they are cantilevered upward. The pendulum was released and the force consumed in breaking the sample calculated from the height the pendulum reached on the flow through. The test specimen was prepared by matching operation. Five specimens were tested for each sample.

2.10 Water absorption studies

The water absorption measurements of tetra glycidyl epoxy were carried out according to ASTM D570-81 was immersed in water for 24h at 25 °C and the percentage of water absorbed by the specimen was calculated using the following equation (2).

$$\% \text{ water absorption} = (W_2\text{-}W1) \times 100/W_1 \quad (2)$$

Where,

W_1 is the initial weight of the sample and

W_2 is the weight of the sample after immersion in water for 24 h at 25°C.

3.0 Results and discussion

FT-IR spectra were used to elucidate the functional groups present in the TGBAPSB epoxy resin before and after reinforcement with F-nAl. FT-IR spectrum of functionalized F-nAl is shown in Fig. S1. The absorption peak at 3362 cm^{-1} was attributed to NH_2 groups. The peaks

at 2919 and 2844 cm^{-1} were assigned to the symmetric methylene (CH_2) stretching vibrations respectively. The presence of bands at 1580 (NH), 1417 (CH) and 1148 (C-N) are due to stretching and bending vibrations. The FTIR spectrum of BNPSB is presented in Fig. S2. The appearance of bands at 2836 (Ar-CH), 1586 (C=C), 1491 (C-O-C), 1153 (Ar-NO_2), 1322 (S=O), 741 (C-S) and 842 (C-N). The disappearance of nitro group at 1153 cm^{-1} and appearance of peak at 3475 due to NH_2 are also shown in Fig.S2 (a) and (b). In Fig. 3 (a), the band at 912 cm^{-1} appears due to the presence of oxirane ring. The bands appeared at 2975 cm^{-1} and 1650 cm^{-1} represent the aromatic ring of TGBAPSB and 821 cm^{-1} for the C-N stretching of TGBAPSB. The disappearance of peak at 912 cm^{-1} and appearance of peak at 3340 cm^{-1} represent the opening of oxirane ring and formation of for secondary hydroxyl group respectively. Fig. 3 (b) confirm the reaction occurred between epoxy and DDM. Having elucidated the functional groups, it is a requisite to understand the structural characteristics of the synthesized TGBAPSB epoxy resin. Therefore, ^{1}HNMR was employed to interpret the chemical structure of TGBAPSB epoxy resin. Fig. S4 illustrates ^{1}HNMR spectrum of BNPSB. The appearance of chemical shifts at around (m, 16H, ArH) 6.5-7.9 ppm, confirmed the presence of aromatic protons. Fig. S5 shows the ^{13}CNMR spectrum of BNPSB. The peaks at 141, 114, 123, 162, 163, 117, 130 and 134 (C aromatic) are assigned to the aromatic carbons of BNPSB. Fig. S6 illustrates the ^{1}HNMR spectrum of BNPSB. The appearance of chemical shifts around 6.5-7.9 (m, 16H, ArH) confirmed the presence of aromatic protons and the appearance of di-amine chemical shifts occurred at (s, 4H, $ArNH_2$) 3.9 ppm. Fig. S7 shows the ^{13}CNMR spectrum of BAPSB. The peaks at 143, 123, 116, 147, 164, 114, 130 and 135 (C aromatic) are assigned to the aromatic carbons of BAPSB. Fig. S8 illustrates the ^{1}HNMR spectrum of TGBAPSB epoxy resin. The chemical shift values obtained are assigned according to the protons of their environment; 6.5-7.9 ppm (m, 16H, ArH) indicating the presence of aromatic protons. The remaining methyl, oxirane, and methylene protons appear at around 2.5 (s, 8H, CH_2), 3.2-3.7 (d, 12H, CH_2) respectively. Fig. S9 depicts the ^{13}CNMR spectrum of TGBAPSB. The appearance of signals respectively at δ=45 ppm and 50 ppm are assigned due to the presence of $–OCH_2$ and –CH– of TGBAPSB epoxy resin. The signal at δ=59-60 is assigned to the presence of $–N–CH_2$ carbon. The remaining signals that appear respectively at δ 109ppm, 116ppm, 127ppm, 144ppm, 148ppm and 165ppm (C aromatic) are assigned to the aromatic carbons of TGBAPSB. Fig. S10 shows the GPC graph

of TGBAPSB epoxy with a number average molecular weight ($\overline{M}_n$) 775, weight average molecular weight ($\overline{M}_w$) 813 and poly dispersity index ($\overline{M}_w/\overline{M}_n$) 1.04.

3.1 Mechanical properties

The nanocomposites are expected to possess improved toughness, better mechanical properties than the neat TGBAPSB epoxy resin. The improvement in mechanical properties was ascertained analyzing the tensile strength, flexural strength and impact strength of neat and nanocomposites. The values of tensile strength, flexural strength and impact strength of neat and nanocomposites are presented in Table S2. A significant enhancement in tensile strength, flexural strength and impact strength was observed when F-nAl was introduced into the epoxy matrix. It was also interesting to note that the 1wt% (system 'b') and 3wt% (system 'c') of F-nAl reinforced nanocomposites systems exhibited the ideal values of mechanical properties in terms of tensile strength, flexural strength and impact strength and are shown in Fig. 11. For instance, the values of tensile, flexural and impact strength of system 'c' (3 wt%) are 124.5 MPa, 212.5 MPa and 238.4 J/m respectively, when compared to those of neat TGBAPSB (system 'a'). This may be due to the formation of strong covalent bond between epoxy and F-nAl nanoparticles through silane linkage. Similar observation was made by Laura et al (2008) for mechanical, and fracture properties of alumina based epoxy nanocomposites.[22] In the case of higher concentration loading of F-nAl (5wt %) reinforced nanocomposite system 'd' the mechanical properties were found to be decreased. This could be attributed to the irregular dispersion of the alumina nanoparticles within the epoxy matrix thereby creating a void of cross-linking. This void of crosslinking paves an avenue for the molecular relaxation and consecutive segmental mobility of the polymer chains. This is well supported by the value of T_g observed for the system 'd' from the DMA analysis. This may be considered as one of the reasons for the decrease in mechanical properties of the 5wt% (system 'd') F-nAl nanocomposites. Similar phenomenon was reported by Mohanty et al (2013) for aggregation resulting from high loading of alumina in epoxy nanocomposites.[23] The increasing and decreasing trend of values of mechanical properties with respect to nanoreinforcement loading may also be attributed to the uniform and irregular dispersion the F-nAl in the TGBAPSB epoxy matrices. This could be correlated with the SEM analysis observations, which clearly indicates that the surface roughness

increases at higher loading of F-nAl into the TGBAPSB epoxy matrix system ‘d’ which exhibits irregular dispersion. Thus, it could be concluded that the mechanical properties of systems ‘b’ and ‘c’ having proper distribution of F-nAl which is brought about only at a lower loading of F-nAl namely 1 and 3wt% exhibit an increasing trend.

3.2 Dynamic mechanical analysis (DMA)

The results of DMA of TGBAPSB (neat) epoxy resin and (1-5wt %) F-nAl reinforced TGBAPSB epoxy nanocomposites are shown in Fig. 12 and Table S3. It can be observed that the storage modulus (E´) increases for nanocomposites systems ‘b’ and ‘c’, which is higher than that of the neat TGBAPSB epoxy system ‘a’. However, the maximum improvement in storage modulus is observed for nanocomposites up to 3wt% of F-nAl system ‘c’. The nanocomposites system ‘d’ has exhibited a least value of storage modulus when compared to that of nanocomposites systems ‘b’ and ‘c’. The increase in storage modulus observed upto 3 wt% (system ‘c’) of all F-nAl reinforced systems may be due to the uniform dispersion of nanoalumina particles within the epoxy matrix.[23] During the curing process, the DDM reacts with epoxy and F-nAl forming covalent bond between reinforcement and matrices. The decrease in storage modulus observed for system ‘d’ (beyond 3wt% of F-nAl loading) is mainly attributed to irregularly dispersed F-nAl particles into the epoxy matrix and in turn the void of cross-linking is increased. Hence the segmental mobility rises, which leads to the decrease of the storage modulus. On the other hand, the neat TGBAPSB (system ‘a’) showed the least storage modulus (3.2GPa) among all the systems ‘b’ and ‘c’. This may be due to the presence of the flexible ether and sulphone linkages of TGBAPSB epoxy resin.[24] The increase in storage modulus up to 3wt% loading of F-nAl TGBAPSB epoxy nanocomposites may also be attributed to the homogenous dispersion of the F-nAl in the epoxy matrix system ‘c’. However, at higher loading of F-nAl (5wt%) a decreasing trend was observed for system ‘d’, which could be attributed to the irregular dispersion of F-nAl particles in the TGBAPSB epoxy matrix. These observations are in concurrence with those results of mechanical properties of TGBAPSB epoxy nanocomposites where higher loading of 5wt% resulted in a negative feedback on the mechanical and morphological characteristics.

3.3 Glass transition temperature (T_g)

Glass transition temperature (T_g) was determined from the peak position of tan δ, which increased from 145 to 203°C with increasing nanoalumina content as shown in Fig. 13 and the values of T_g are given in Table 3. The T_g of neat TGBAPSB epoxy resin was found to be the least (145°C) among all the systems investigated. It was interesting to note that the T_g of nanocomposites (systems 'b' and 'c') increased steadily up to 3wt% of F-nAl incorporation. The increasing T_g observed for 'b' and 'c' systems may be due to the increase in storage modulus resulting from the uniform dispersion of alumina nanoparticles within the epoxy matrix and thus offering stiffening effect with the presence of alumina and silane components of F-nAl that tightly holds the TGBAPSB epoxy matrices in a cross-linked structure by restricting the mobility of epoxy resin chain segments.[25,26] However, the T_g value of system 'd', decreases due to the aggregation of alumina nanoparticles at higher (5wt%) concentration of F-nAl.[27]

3.4 Thermo gravimetric analysis

The thermal degradation behavior of neat and nanocomposites are presented in Fig. 14 and Table 4. The thermal stability and char yield TGBAPSB systems are improved up to 3wt% loading of nanoreinforcements. For example the initial decomposition of TGBAPSB system 'a' occurred at 330°C while the initial decomposition temperatures of system 'a' and system 'b' shown in Table 4 were significantly improved to 337°C and 349°C respectively. Similarly the char yield of system 'a' was 16% and that of the system 'b', system 'c' were enhanced to 21% and 31% respectively. The TGA curve of 3wt% (system 'c') loaded alumina nanocomposite indicates an improved thermal stability than that of the 5 wt% (system 'd') alumina reinforced nanocomposites, which showed a reverse trend in stability and are presented in Fig. 14. This could be attributed to the uniform dispersion of nanoalumina particles within the nanocomposites. However, the aggregation of higher loading of 5wt% of nanoalumina leads to reduced thermal stability, which is indicated by its initial degradation and char yield in comparison with that of 3wt% loaded system.[23] It was interesting to observe that the increase in weight percentages (1, 3 and 5wt%) of F-nAl in the TGBAPSB epoxy systems namely 'b', 'c' and 'd', prolonged the initial degradation temperature of the TGBAPSB nanocomposites when

compared to that of neat TGBAPSB epoxy matrix system 'a'. This enhancement in thermal stability could be ascribed to the presence of inorganic materials like alumina (Al) and silane (Si) components of F-nAl into the epoxy network.

3.5 Differential scanning calorimetry (DSC)

The values of the glass transition temperature (T_g) of neat epoxy matrix and nanoalumina reinforced nanocomposites were obtained from the DSC analysis are also presented in Table 4. The values of T_g of neat TGBAPSB (system 'a') was 148°C whereas the values of T_g of nanocomposites system 'b', system 'c' and system 'd' are 189°C, 205°C and 180°C respectively (Fig. 15). These results are in good agreement with the tan δ (T_g) values resulted from DMA studies (Table 4). The increasing and decreasing T_g value observed for systems 'b', 'c', 'd' and 'a' from both DMA and DSC studies could be mainly due to the uniform and non-uniform dispersion of F-nAl within the epoxy matrix.

3.6 XRD and TEM studies

XRD diffraction (XRD) analysis was carried out for the neat TGBAPSB and epoxy reinforced with different weight percentages of F-nAl and the results are illustrated in Fig. 16. The Fig. 16 illustrates the variation in the peak intensity of F-nAl filled TGBAPSB epoxy nanocomposites from 2θ=16.2º to 2θ =13.2º respectively. It can be clearly seen that the peak intensity significantly reduced up to 3wt% (systems 'b' and 'c'). The shift towards a lower angle indicates that the interplanar spacing was decreased and indicating that the mixed intercalated and exfoliated behavior of the epoxy nanocomposites,[28,29] when compared to that of neat TGBAPSB epoxy matrix and are shown in Fig. 16. The decrease in interplanar spacing was more in the case of system 'd' than the other systems namely 'b' and 'c'. This trend clearly indicates that the systems 'b' and 'c' have more exfoliated character than system 'd'. The introduction of F-nAl at lower concentrations led to its proper dispersion within the TGBAPSB epoxy systems 'b' and 'c' (Fig. 17a) and thus showing more exfoliation than system 'd'. However, higher weight percentage loading (system 'd') of nanoalumina particles with epoxy resin had strong tendency of nanoalumina particles to agglomerate within the resin and thus led to a decreased

interplanar spacing.[27] The decreased interplanar spacing observed for system 'd' having higher loading of nanoparticles can be attributed to the inevitable occurrence of aggregates, which was confirmed by TEM image (Fig. 17b).

3.7 Morphology of the nanocomposites

Fig. 18 show the SEM and AFM micrographs of TGBAPSB (neat) epoxy (system 'a') and nanocomposites (systems 'b, 'c' and 'd'). It was observed that the surface of TGBAPSB (neat) epoxy was smooth (Fig. 18a). However, on addition of F-nAl particles, the surface morphology of the epoxy nanocomposites 'b', 'c' and 'd' was found to be rough in nature and the surface roughness increases up to 3wt% of nanoalumina concentration. There is an excellent adhesion due to the formation of chemical bond between the nanoalumina and the epoxy resin and hence, there is a formation of a partially intercalated and exfoliated structure. This effect results in improved strength of the nanocomposites namely 'b' and 'c' systems (Fig. 18b and c).[30] Furthermore, addition of 5wt% of nanoalumina reinforced nanocomposites system 'd' possesses crack initiation sites due to the presence of aggregates of nanoalumina particles and this eventually result in the cutback of storage modulus. Similar observations were made from DMA and mechanical studies where 5wt% F-nAl reinforced nanocomposites exhibited depletion in storage modulus due to the aggregation of excess nanoalumina particles (Fig. 18 d).[29] Furthermore, the TEM images also support the observation made from AFM, SEM, DMA and mechanical studies.

3.8 Dielectric behavior

The values of dielectric constant of neat and nanoalumina reinforced epoxy composites are shown in Table 5. Dielectric constant is a property of an electrical insulating material (a dielectric) equal to the ratio of the capacitance of a capacitor filled with the given material to the capacitance of an identical capacitor in a vacuum without the dielectric material. An excellent insulator should have low dielectric electric constant values. It was noted that the incorporation of F-nAl in to the TGBAPSB epoxy reduces the dielectric constant values. The values of dielectric constant are decreased with an increase in the content of the

F-nAl in the epoxy matrix. For example the dielectric constant of neat TGBAPSB epoxy matrix system was 4.00, whereas the dielectric constant of epoxy nanocomposites systems 'b', 'c' and 'd' were 3.85, 3.60 and 3.55 respectively. This may be attributed to the increased interfacial areas created by the F-nAl during the formation of nanocomposites. These results are in concurrence with those reported by Gonon et al (2001).[31] These results indicate that reinforcing F-nAl, into the TGBAPSB epoxy matrix increases the insulating property besides having the better influencing effect at lower loading and impact on the insulation properties.

3.9 Water absorption properties

Water absorption properties also followed the same trend as thermo-mechanical properties where the values decreased with increasing F-nAl content. The values of water absorption properties of neat and nanoalumina reinforced epoxy composites are shown in Table 5. It can be seen from Table 5 that the water absorption gradually decreased with an increase in the F-nAl content. For example, the percentage of water absorption of the system 'a' was 0.067, whereas the same for the systems 'b', 'c' and 'd' were found to 0.064, 0.062 and 0.061 respectively. This could have been caused by two factors. Firstly, the volume of epoxy for water diffusion is reduced with increasing nanoparticle content. Secondly, the presence of nanoparticles can increase the path length for moisture diffusion as reported by Ng et al (2001).[32]

4 Conclusions

Novel skeletally modified sulphone tetra functional epoxy nanocomposites were successfully developed using TGBAPSB epoxy resin and surface modified F-nAl. The surface morphology of the epoxy nanocomposites was investigated by XRD, TEM, SEM and AFM studies. It was interesting to observe that the XRD patterns of 1wt%, 3wt% and 5wt% loaded F-nAl TGBAPSB nanocomposites exhibited mixed intercalated and exfoliated behavior than the neat one. The percentage of exfoliation is more in the case of 1% and 3wt% loaded system than 5wt% loaded one. This is indicative of effective dispersion of F-nAl within epoxy, which could be achieved only at low weight percentage. Surface morphological results from SEM, TEM and AFM show that the 3wt% loaded F-nAl TGBAPSB nanocomposites exhibit mono dispersity

while 5wt% loaded F-nAl TGBAPSB nanocomposites exhibit aggregation. It was also observed that upon comparing the tensile, flexural and impact properties of neat and F-nAl reinforced composite systems, a beneficial increase in mechanical properties for the reinforced composite systems was observed. The nanoreinforcement (F-nAl) produced a significant improvement on the thermal stability and char yield of the TGBAPSB tetra functional epoxy system. The TGBAPSB epoxy matrix showed the least value of dielectric constant indicating that the best insulation properties. Thus the TGBAPSB epoxy resin reinforced with optimized F-nAl loading possess better mechanical, thermal and thermo mechanical insulation characteristic than those of conventional and di-functional epoxy materials. Hence the material development in the present work could be explored for a possible high performance and industrial applications that require improved durability.

Acknowledgements

Instrumentation facility provided under FIST-DST and DRS-UGC to Department of chemistry, Anna University, Chennai are grate fully acknowledged.

Supplementary file

Fig. 1. FT–IR spectra of F-nAl

Fig. 2. FT-IR spectra of (a) BNPSB (b) BAPSB

Fig. 4. ^{1}HNMR spectra of BNPSB

Fig. 5. ^{1}HNMR spectra of BAPSB

Fig. 6. ^{1}HNMR spectra of TGBAPSB epoxy resin

Fig. 7. ^{13}CNMR spectra of BNPSB

Fig. 8. ^{13}CNMR spectra of BAPSB

Fig. 9. ^{13}CNMR spectra of TGBAPSB epoxy resin

Fig. 10. GPC of TGBAPSB epoxy resin

Table 1 Nomenclature of TGBAPSB epoxy nanocomposites

Table 2 Data on mechanical properties of TGBAPSB epoxy nanocomposites

Table 3 DMA results of TGBAPSB epoxy nanocomposites

References

1. M. S. Bhatnagar, *Polym. Plast. Technol.,* 1993, **32,** 53.
2. S. Bhuniya and B. Adhikari, *J. Appl. Polym. Sci.,* 2003, **90,** 1497.
3. J. Lee and A. F. Yee, *Polymer,* 2001, **42,** 577.
4. J. Frohlich, R. Thomonn and R. Mulhaupt, *Macromolecules,* 2003, **36,** 7205.
5. J. Y. Lee, M. J. Shim and S. W. Kim, *J. Appl. Polym. Sci.,* 2001, **81,** 479.
6. S. J. Park and H. C. Kim, *J. Polym. Sci. Part B. Polym. Phy.***,** 2000, **39,** 121.
7. A. Bonnet, J. P. Pascault and H. Sautereau, *Macromolecules***,** 1999, **32,** 8524.
8. H. K. Kim and K. H. Char, *Ind. Eng. Chem.,* 2000, **39,** 955.
9. X. Z. Song, S.X. Zheng, J. Y. Huang, P. P. Zhu and Q. P. Guo, *J. Appl. Polym. Sci.,* 2001, **79,** 598.
10. A. Zudeldia, M. Larranga, P. Remiro and I. Mondragon, *J. Polym. Sci. Part B. Polym. Phy.*, 2004, **42,** 3920.
11. S. Ananda Kumar and Z. Denchev, *Prog. Org. Coat.,* 2009, **66,** 1.
12. G. Kamlesh, Amin, P. Manish, Patel, G. Ranjan and Patel, *Die Angewandte Makromole kulare Chemie,* 1999, **266,** 46.
13. F. Mustata and I. Bichu, *J. Appl. Polym. Sci.,* 2000, **77,** 2430.
14. S. Ritzenthaler, F. Court, L. David, E. Girard-Reydet, L. Leibler and J.P. Pascault, *Macromolecules,* 2002, **35,** 6245.
15. V. Rebizant, V. Abetz, F. Tournilhac, F. Court and L. Leibler, *Macromolecules,* 2003, **36,** 9889.
16. T.J. Hermel-Davidock, H.S. Tang, D.J. Murray and S.F. Hahn*, J. Polym. Sci. Part. B: Polym. Phys.,* 2007, **45,** 3338.
17. F. Yi, S. Zheng and T. Liu, *J. Phys. Chem. B.,* 2009, **113,** 1857.
18. S. Dharmendra Kumar, V. Subramanyam, Kasisomayajula and P. Venkitanarayanan, *Compos. Sci. Technol.,* 2008, **68,** 3055.
19. R.A. Sharma, D. D'Melo, S. Bhattacharya, L. Chaudhari and S. Swain, *Trans. Electric. Electro. Mater.,* 2012, **13,** 31.

20. D. Duraibabu, T. Ganeshbabu, R. Manjumeena, S. Anandakumar and D. Priya, *Prog. Org. Coat.,* 2013, **77,** 657.
21. Y. Jinhong, H. Xingyi, W. Lichun, P. Peng, W. Chao, W. Xinfeng and Pingkai, *J. Polym. Chem.,* 2011, **2,** 1380.
22. M. Laura, McGrath, S.P. Richard, K.H. Saskia, L.S. John, A.F. Daniel, L. Joseph and Lenhart, *Polymer.,* 2008, **49,** 999.
23. Akash, Mohanty and V.K. Srivastava, *Materials and Design,* 2013, **47,** 711.
24. D. Ratna, M. Patri, B.C. Chakraborty and P.C. Deb, *J. Appl. Polym. Sci.,* 1997, **65,** 901.
25. Y. Zhou, F. Pervin, L. Lewis and S. Jeelani, *Mater. Sci. Eng. A.,* 2007, **452,** 657.
26. Y. Zhou, F. Pervin, V.K. Rangari and S. Jeelani, *Mater. Sci. Eng. A.,* 2006, **426,** 221.
27. B. Akbari and R. Bagheri, *Eur. Poly. J.,* 2007, **43,** 782.
28. S. Zainuddin, M.V. Hosur, Y. Zhou, Alfred, T. Narteh, Ashok Kumar and S. Jeelani, *Mater. Sci. Eng. A.,* 2010, **527,** 7920.
29. S. Zainuddin, M.V. Hosur, Y. Zhou, A. Kumar and S. Jeelani, *Mater. Sci. Eng. A.,* 2009, **507,** 117.
30. C.L. Wu, M.Q. Zhang, M.Z. Ron and K. Friedrich, *Comp. Sci. tech.,* 2002, **62,** 1327.
31. P. Gonon, A. Sylvestre, J. Teysseyre and C. Prior, *Mater. Sci. Eng. B.,* 2001, **83,** 158.
32. C.B. Ng, B.J. Ash, L.S. Schadler and R.W. Siegel, *Adv. Compos. Mater.,* 2001, **10,** 101.

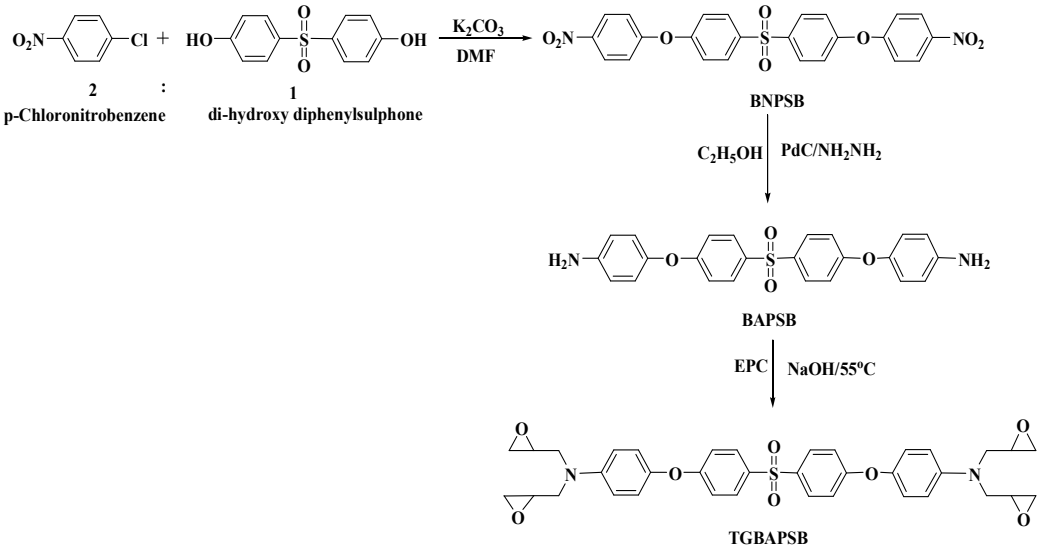

Scheme 1 Synthesis of TGBAPSB epoxy resin

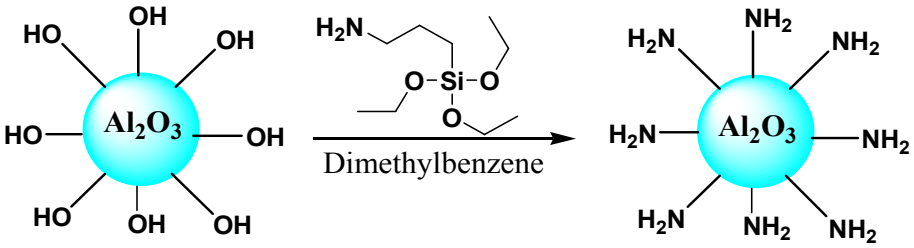

Scheme 2 Amino functionalized nanoalumina

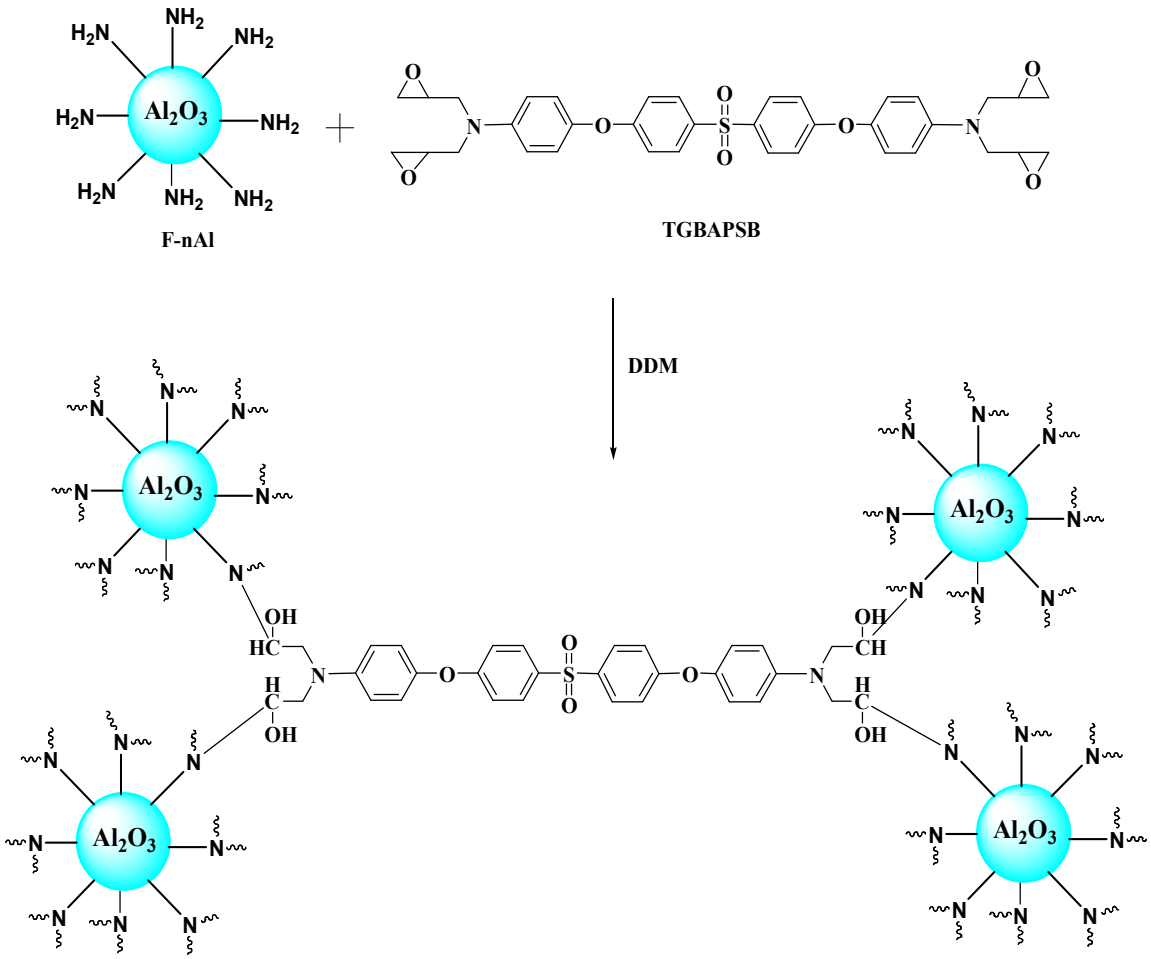

Scheme 3. The reaction mechanism of TGBAPSB with F-nAl nanoparticle

Table 4

Data on thermal properties of TGBAPSB epoxy nanocomposites

System	TGBAPSB/% F-nAl	Initial Decomposition Temperature (ºC)	Char yield (%)	T_g (ºC)
a	100/0	330	16	148
b	100/1	337	21	189
c	100/3	349	31	205
d	100/5	345	26	180

Table 5

Dielectric properties and water absorption of TGBAPSB epoxy nanocomposites

System	TGBAPSB/% F-nAl	Dielectric Constant (ε')	Water absorption (%)
a	100/0	4.00	0.067
b	100/1	3.85	0.064
c	100/3	3.60	0.062
d	100/5	3.55	0.061

Figure captions

Fig. 3. FT-IR spectra of (a) TGBAPSB epoxy resin (b) TGBAPSB epoxy resin cured with DDM

Fig. 11. Mechanical properties of neat (TGBAPSB) and F-nAl epoxy nanocomposites

Fig. 12. Storage modulus of neat (TGBAPSB) and F-nAl epoxy nanocomposites

Fig. 13. Tan δ of neat (TGBAPSB) and F-nAl epoxy nanocomposites

Fig. 14. TGA of neat (TGBAPSB) and F-nAl epoxy nanocomposites

Fig. 15. DSC of neat (TGBAPSB) and F-nAl epoxy nanocomposites

Fig. 16. XRD spectra of (a) neat (b) TGBAPSB/1wt% Fn-Al, (b) TGBAPSB/3wt% Fn-Al and (d) TGBAPSB/3wt% Fn-Al epoxy nanocomposites

Fig. 17. TEM photographs of systems (a) TGBAPSB/3wt% Fn-Al and (b) TGBAPSB/5wt% Fn-Al epoxy nanocomposites

Fig. 18. SEM and AFM photographs of systems (a) TGBAPSB neat (b) TGBAPSB/1wt% Fn-Al (c) TGBAPSB/3wt% Fn-Al epoxy nanocomposites and (d) TGBAPSB/5wt% Fn-Al